Experimental Study of NO Reaction with Isoprene Hydroxyalkyl Peroxy Radicals

Dan Zhang,[†] Renyi Zhang,*[,†] and Simon W. North[‡]

Department of Atmospheric Sciences, Department of Chemistry, Texas A&M University, College Station, Texas 77843

Received: July 11, 2003; In Final Form: September 12, 2003

Despite the importance of isoprene hydroxy peroxy radicals (RO_2) in the conversion of NO to NO_2 and hence in tropospheric ozone formation, no direct experimental studies have been carried out to investigate the kinetics of the RO_2−NO reaction. We report the first direct laboratory study of the rate constant for the isoprene RO_2−NO reaction using a fast-flow reactor coupled to chemical ionization mass spectrometry (CIMS) detection. By directly monitoring the peroxy radical, a rate constant of $(9 \pm 3) \times 10^{-12}$ cm^3 molecule^{-1} s^{-1} was determined in the pressure range of 1 to 2 Torr and at a temperature of 298 ± 2 K. The measured rate constant is compared to the results of a recent theoretical prediction and indirect measurements and implications for the atmosphere are discussed.

1. Introduction

Isoprene (2-methyl-1,3-butadiene, $CH_2{=}C(CH_3)CH{=}CH_2$) is one of the most abundant hydrocarbons emitted by the terrestrial biosphere, with a global averaged annual production of approximate 450 Tg.[1] Because of its high chemical reactivity and proliferation in the generation of peroxy radicals,[2] oxidation of isoprene plays an important role in tropospheric ozone production on the regional scale.[3,4] Atmospheric oxidation reactions of isoprene can be initiated by hydroxy radicals (OH), ozone (O_3), nitrate radicals (NO_3), or halogen radicals (Cl or Br).[5] Since isoprene is mainly emitted from vegetation during the daytime, the reaction of isoprene with OH is expected to be the dominant tropospheric removal pathway. The initial reaction between isoprene and OH proceeds exclusively by OH addition to the >C=C< bonds, yielding an OH−isoprene adduct, the hydroxyalkyl radical[6]

$$C_5H_8 + OH\bullet \rightarrow C_5H_8OH\bullet \quad (1)$$

Under atmospheric conditions, the hydroxyalkyl radical reacts primarily with the oxygen molecule to form hydroxyalkyl peroxy radical (RO_2),[6]

$$C_5H_8OH\bullet + O_2 \rightarrow C_5H_8OHO_2\bullet \quad (2)$$

Reaction 2 leads to the formation of six possible isomers of the peroxy radicals depending on the position O_2 is being added to the OH−isoprene adduct.[6] Our previous theoretical studies suggest that these isomers have noticeably different yields and reactivities.[6] The degradation products formed from the various isomers of the peroxy radicals are also different.[7]

In the presence of nitric oxide (NO), the resulting hydroxyalkyl peroxy radical reacts with NO, leading to the hydroxyalkyl peroxy nitrite radical intermediate which further undergoes either decomposition to form hydroxyalkoxy radical (major channel) or isomerization to produce organic nitrate (minor channel),[8]

$$C_5H_8OHO_2\bullet + NO \rightarrow C_5H_8OHOONO\bullet$$

$$\rightarrow C_5H_8OHO\bullet + NO_2 \quad (3a)$$

$$\rightarrow C_5H_8(OH)ONO_2 \quad (3b)$$

Reaction 3a is directly responsible for ozone formation, whereas reaction 3b results in NO_x removal and chain termination. It has been suggested that 50−100% of ozone production in some regional areas of the United States is due to reaction 3a.[9] As much as 7% of NO produced from fossil fuel combustion in North America in the summer is lost as nitrates formed because of reaction 3b.[10] In addition, the isoprene nitrates are responsible for about 4% of nitrogen oxides transported from North America.[11] Hence, the isoprene RO_2–NO reaction represents one of the most central chemical reactions of substantial tropospheric impact.

Numerous laboratory studies have been conducted to investigate the kinetics and mechanism of the OH-initiated reactions of isoprene.[2,12−18] The majority of the previous studies investigated either the initial step of the OH−isoprene reaction chain[12] or the final reaction products.[16,17] For example, several experimental studies have reported the organic nitrate yield from the OH-initiated oxidation of isoprene, ranging from 4 to 13%.[10,16,17]

Direct experimental data concerning the intermediate processes of the isoprene reactions are, however, very limited. Jenkin et al. investigated the permutation reactions (i.e., self- and cross-reactions) of the isoprene hydroxy peroxy radicals using the laser flash photolysis/UV absorption spectrometry technique.[19] Recent experimental studies have investigated OH cycling from the OH−isoprene reactions in the presence of NO, in an attempt to indirectly infer the fate of isoprene hydroxyalkyl peroxy and alkoxy radicals.[13,14] We have investigated the hydroxyalkyl radicals and their corresponding peroxy radicals arising from the OH-initiated reactions of isoprene using a fast-flow reactor coupled to chemical ionization mass spectrometry (CIMS) detection.[12,15] On the basis of observation of the peroxy radicals, direct kinetic measurements of the reaction between hydroxyalkyl radicals and O_2 were performed.[15] In addition, we have performed theoretical studies of the isoprene RO_2−NO reaction, using density functional theory (DFT) and ab initio molecular orbital calculations along with kinetic rate theories.[8]

* Address correspondence to this author.
[†] Department of Atmospheric Sciences.
[‡] Department of Chemistry.

10.1021/jp0360016 CCC: $25.00
Published on Web 11/18/2003

Our theoretical study indicates that the entrance and exit channels of the RO_2-NO reaction were barrierless and the rate constants for the RO_2 isomers to form ROONO were calculated to be in the range of 3×10^{-12} to 2×10^{-11} cm^3 molecule^{-1} s^{-1} using the canonical variational transition state theory (CVTST).[8] In addition, kinetic studies of other C1−C5 alkyl peroxy radicals with NO yielded the rate constants in the range of $(7.5-10.9) \times 10^{-12}$ cm^3 molecule^{-1} s^{-1},[20] and the commonly adopted rate constant for the RO_2-NO reaction is 7.6×10^{-12} cm^3 molecule^{-1} s^{-1} in atmospheric model studies.[2,7]

In this paper, we report a direct experimental kinetic study of the reaction of NO with hydroxyalkyl peroxy radicals arising from the OH-initiated reactions of isoprene. The isoprene peroxy radicals were produced in a fast-flow reactor in the presence of OH, isoprene, and O_2. The reactants (OH and isoprene) and peroxy radicals were detected by using chemical ionization mass spectrometry (CIMS). The experimental kinetic results are compared to our recent theoretical predictions of the isoprene RO_2-NO reaction using quantum-chemical methods and kinetic rate theories.

2. Experimental Section

A fast-flow reactor, in conjunction with chemical ionization mass spectrometry (CIMS) detection, was used in the experiments. The detailed experimental apparatus and procedures have been described elsewhere.[12,15,21,22] Briefly, the flow reactor consisted of a Pyrex tubing of 1.225 cm internal diameter and 80 cm in length. All surfaces exposed to the reactants and products were coated with halocarbon wax to reduce the radical wall loss. A flow of N_2 carrier gas in the range of 1−3 L min^{-1} at standard temperature and pressure (STP) was injected into the flow reactor through an entrance port in the rear of the flow reactor. The pressure of the flow reactor was regulated between 1 and 2 Torr and the temperature of all experiments was maintained at 298 ± 2 K. Typical flow velocity in the flow reactor ranged from 1300 to 2500 cm s^{-1}. A high-capacity mechanical pump (1000 *l* min^{-1}) was used to evacuate the flow reactor. Pressures in the flow reactor were monitored by a capacitance manometer near the exit of the flow reactor. Isoprene was added to the flow reactor through a movable injector made of a 3.2 mm outer diameter Pyrex tube. The flow reactor was operated under the laminar flow condition with the Reynolds number $\mathrm{Re} = 2au\rho/\mu$ typically in the range of 70−120, where a is the internal radius of the flow reactor in cm, ρ the density of the gas (in g cm^{-3}), u the flow velocity (in cm s^{-1}), and μ the absolute viscosity of the gas (in g cm^{-1} s^{-1}). The entrance length required for the flow to fully develop a parabolic velocity profile (laminar flow) was estimated using $l = 0.115a\mathrm{Re}$,[23] which gives the central velocity to attain 99% of its final value. Using a typical value of 80 for the Reynolds number under our experimental conditions, this length was determined to be about 11.3 cm, significantly shorter than that of the flow reactor. The mixing times for isoprene and OH were estimated by using $t_{mix} = a^2/(5D_c)$,[23] where D_c is determined by the pressure-independent diffusion coefficient, pD_c. At 298 K, the values of pD_c are 228 Torr cm^2 s^{-1} for OH and 111 Torr cm^2 s^{-1} for isoprene in nitrogen gas, and the mixing lengths are 5.3 and 10.8 cm for these two species, respectively. A laminar flow was fully developed and homogeneous mixing of both OH and isoprene was effectively achieved under our experimental conditions.

Reactants and products of the OH−isoprene reaction were detected by CIMS using either positive or negative reagent ions. The CIMS employs a new approach, involving an electrostatic ion guide.[24,25] Gases from the flow reactor were introduced into the ion−molecule reaction region. Positive or negative reagent ions were initiated using a corona discharge at a high voltage (±5 kV). The SF_6^- reagent ions were generated by adding a small amount of SF_6 gas to a N_2 carrier flow (about 1−2 slpm at STP) through the discharge. The positive reagent ions O_2^+ were produced by passing a He carrier flow through the discharge and then adding a small amount of O_2 downstream. A small portion of the ion/gas flow from the ion source was drawn into the next vacuum stage through a 0.5 mm orifice. An electrostatic ion guide was used to transport ions to another orifice leading to the quadrupole mass analyzer. Two turbomolecular pumps were used to evacuate the chambers housing the ion guide and the mass spectrometer. The use of the ion guide allows for ion transportation with a high efficiency and preferential separation and removal of neutral molecules in a differential pumping system.[24,25] Detection sensitivity of the present CIMS system was generally in the range of 10^6 to 10^7 molecules cm^{-3} with an S/N ratio of unity for a one second integration time, independent of pressure.

OH radicals were generated in situ according to the reaction[26]

$$\mathrm{H} + \mathrm{NO_2} \rightarrow \mathrm{NO} + \mathrm{OH} \qquad (4)$$

Hydrogen atoms were generated by passing a small flow of a 1% H_2/He mixture (about 0.5 cm^3 min^{-1} at STP) through a microwave discharge. OH radicals were produced by addition of an excess of a 1% NO_2/N_2 mixture. Typical NO_2 concentrations in the flow reactor were in the range of $(3-7) \times 10^{11}$ molecule cm^{-3}. OH was detected in the negative ion mode using SF_6^- reagent ion, according to the ion−molecule reaction[12]

$$\mathrm{OH} + \mathrm{SF_6^-} \rightarrow \mathrm{OH^-} + \mathrm{SF_6} \qquad (5)$$

The procedure to calibrate OH was similar to those described previously.[12] The OH concentration was obtained by comparing the relative signal intensities between OH (S_{OH}) and NO_2 (S_{NO2}) followed by a calibration of NO_2 in CIMS, using the relation

$$[\mathrm{OH}] = k_7 S_{\mathrm{OH}} [\mathrm{NO_2}]/(k_5 S_{\mathrm{NO2}}) \qquad (6)$$

where k_5 and k_7 are the ion−molecule reaction rate constants for reactions 5 and 7, respectively.

$$\mathrm{NO_2} + \mathrm{SF_6^-} \rightarrow \mathrm{NO_2^-} + \mathrm{SF_6} \qquad (7)$$

Typically, the initial concentrations of OH in the flow reactor were in the range of $(5-9) \times 10^9$ molecule cm^{-3}. Commercially available isoprene (Aldrich 99.5%) was used to volumetrically prepare a 2-L glass bulb of a 1% isoprene/He mixture and introduced into the flow reactor using a 10 sccm flow meter. The concentrations of isoprene in the flow reactor were regulated in the range of 5×10^{11} to 2×10^{12} molecule cm^{-3}. Isoprene was detected by the CIMS using positive reagent ions (O_2^+) at its parent ion peak.[27]

To generate the $OH-O_2$-isoprene peroxy radical, OH, isoprene and O_2 were simultaneously introduced into the flow system. O_2 was added into the flow reactor along with a N_2 carrier gas. The production of the peroxy radicals was controlled by the initial concentrations of all three reactants as well as the reaction distance. The peroxy radical was detected using the SF_6^- negative reagent ion according to the ion−molecule reaction[15]

$$\mathrm{C_5H_8OHO_2} + \mathrm{SF_6^-} \rightarrow \mathrm{C_5H_8OHO_2^-} + \mathrm{SF_6} \qquad (8)$$

TABLE 1: Summary of Chemical Reactions Used in Kinetic Simulation for the Reaction System Involving OH, Isoprene, O_2, and NO

reaction	k (cm^3 $molecule^{-1}$ s^{-1})[a]
$C_5H_8 + OH \rightarrow C_5H_8OH$	1.0×10^{-10}[b]
$C_5H_8OH + O_2 \rightarrow C_5H_8OHO_2$	7.0×10^{-13}[c]
$C_5H_8OHO_2 + NO \rightarrow C_5H_8OHO + NO_2$	7.9×10^{-12}[d]
$C_5H_8OHO_2 + NO \rightarrow C_5H_8(OH)ONO_2$	1.1×10^{-12}[e]
$C_5H_8OHO \rightarrow CH_2OH + HO_2 +$ products	1.5×10^{5}[f]
$OH + H_2O_2 \rightarrow H_2O + HO_2$	1.7×10^{-12}
$OH + OH \rightarrow H_2O_2$	3.8×10^{-14}[g]
$OH + NO \rightarrow HONO$	4.1×10^{-14}[g]
$OH + NO_2 \rightarrow HNO_3$	1.5×10^{-13}[g]
$C_5H_8 + NO_2 \rightarrow C_5H_8NO_2$	1.8×10^{-19}
$CH_2OH + O_2 \rightarrow HCHO + HO_2$	9.8×10^{-12}
$HO_2 + NO \rightarrow OH + NO_2$	8.5×10^{-12}

[a] Rate constants are from refs 2 and 24 at 298 K and 760 Torr, except noted otherwise. [b] From ref 12. [c] From ref 17. [d] From this work. [e] Assuming a 12% organic nitrate yield (ref 16). [f] In s^{-1}. [g] Termolecular rate constants at 1.86 Torr.

3. Results and Discussions

To examine the kinetic behavior of the RO_2–NO reaction system, several survey experiments were performed. High concentrations of isoprene ($>10^{14}$ molecule cm^3) and O_2 ($>10^{16}$ molecule cm^3) were initially added to the flow reactor in an attempt to drive both reactions 1 and 2 into completion. The decay of the peroxy radical signal was then monitored as the reaction time was successively increased. Under no circumstance did we observe that the decay of the peroxy radical signal followed the pseudo first-order kinetics. There are several plausible factors contributing to this observation. First, the β-alkoxy radicals produced in reaction 3a are expected to undergo rapid decomposition to form carbonyl compounds and respective radical products.[28,29] The consecutive reactions of the radical products produce HO_2 and hence OH in the presence of NO, leading to OH radical regeneration. Second, there exist six possible isomers for the isoprene peroxy radicals, and the kinetics of the RO_2−NO reaction likely exhibits multiexponential behavior.[8,15] Also, high concentrations of the reactants could complicate the ion−molecule reactions in the CIMS system, possibly interfering with the detection scheme of the peroxy radicals.[15] In this experimental study, the concentrations of isoprene were regulated in the range of $(5-30) \times 10^{11}$ molecules cm^{-3} to avoid complicating the ion−molecule chemistry. Hence, we did not attempt to measure the RO_2−NO kinetics under the pseudo first-order approximation. As to be discussed below, we performed the experiments under conditions such that the measurements are sensitive only to the rate constants for reactions 1 and 3, but not to most other reactions. The rate constant for reaction 1 is well established in the literature. Hence, it is feasible to derive a reliable rate constant for reaction 3.

In our previous study, direct observation of the peroxy radical using the CIMS was utilized to obtain the reaction rate constant between the OH−isoprene adduct and O_2.[15] In this study, we have extended this procedure to examine the temporal evolution of the peroxy radical in the presence of NO, to derive a reaction rate constant between the peroxy radical and NO. The experimental and modeling procedures were as follows. The temporal profile of the peroxy radical was measured in the presence of NO by monitoring the peroxy radical signal at mass 117 (corresponding to the $C_5H_8OHO_2^-$ ion), as the injector was successively pulled upstream to increase the reaction time. The observed production of the peroxy radical was then simulated by a kinetic program that included reactions 1, 2, 3a, and 3b, along with other likely secondary reactions. Table 1 lists the reactions and rate constants used in the kinetic simulation. The relevant rate constants were taken from Atkinson et al.[2] and DeMore et al.,[26] except noted otherwise. The rate constants for reactions 1 and 2 were obtained from our previous work.[12,15] Under our experimental conditions, the self-reactions of the isoprene peroxy radicals were unimportant and hence were not included in the kinetic simulation. The total rate constant for reactions 3a and 3b (thereby referred as k_3) was obtained by best fitting the temporal profile of the peroxy radical from the measurements. The branching ratio of $k_{3b}/(k_{3a}+k_{3b})$ was assumed to be 12% as suggested by Tuazon and Atkinson.[16] The model input included the initial concentrations of OH, isoprene, O_2, NO, and all other precursors.

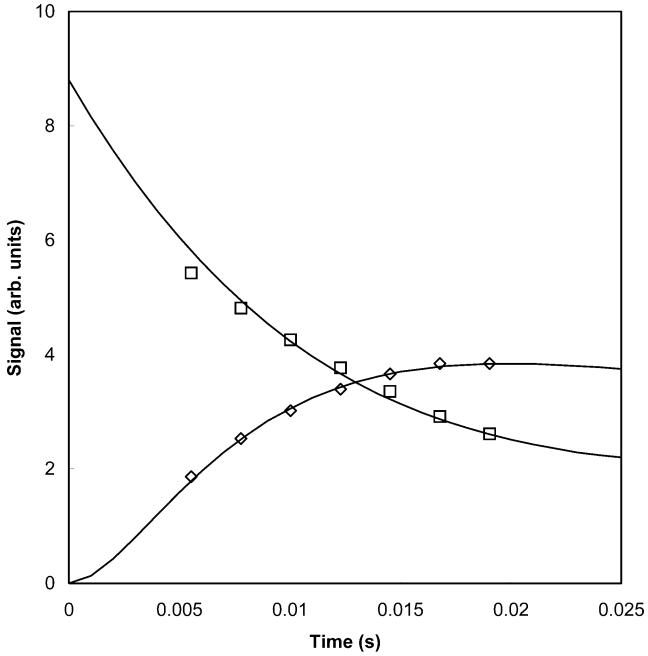

Figure 1. Variation of OH−O_2−isoprene peroxy radical (diamonds) and OH (squares) signals as a function of reaction time. The solid lines represent simulations using a kinetic model (see text). Experimental conditions are $P = 1.86$ Torr, Re = 85, $U = 2258$ cm s^{-1}, $[OH] = 8.8 \times 10^9$ molecule cm^{-3}, $[C_5H_8] = 8.4 \times 10^{11}$ molecule cm^{-3}, $[O_2] = 6.8 \times 10^{14}$ molecule cm^{-3}, and $[NO] = 6.0 \times 10^{12}$ molecule cm^{-3}.

Figure 1 depicts the temporal evolutions of the peroxy radical (diamonds) and OH (squares). The experiment was conducted at 1.86 Torr, and the initial concentrations are $[OH] = 8.8 \times 10^9$ molecule cm^{-3}, $[C_5H_8] = 8.4 \times 10^{11}$ molecule cm^{-3}, $[O_2] = 6.8 \times 10^{14}$ molecule cm^{-3}, and $[NO] = 6.0 \times 10^{12}$ molecule cm^{-3}. The solid lines represent the best fit to the observed formation of the peroxy radical and disappearance of OH. An effective bimolecular rate constant of 9×10^{-12} cm^3 $molecule^{-1}$ s^{-1} was determined for reaction 3, using 7.0×10^{-13} cm^3 $molecule^{-1}$ s^{-1} as the rate constant for reaction 2.

Figure 2 depicts the formation profiles of the peroxy radical at various NO concentrations at 1.86 Torr. The concentrations of all other reactants were maintained constant during the experiments: $[C_5H_8] = 8.4 \times 10^{11}$ molecule cm^{-3}, $[OH] = 8.8 \times 10^9$ molecule cm^{-3}, $[O_2] = 6.8 \times 10^{14}$ molecule cm^{-3}. The top curve represents the peroxy radical formation in the absence of NO. The remaining curves, starting from the second from the top, correspond to the profiles of the peroxy radicals with increasing NO concentrations, ranging from 3.0×10^{12} to 14.4×10^{12} molecule cm^{-3}. There is a noticeable decrease in the intensity of the peroxy radical signal in the presence of increasing NO, indicating the consumption of the peroxy radical because of its reaction with NO. At the highest NO concentra-

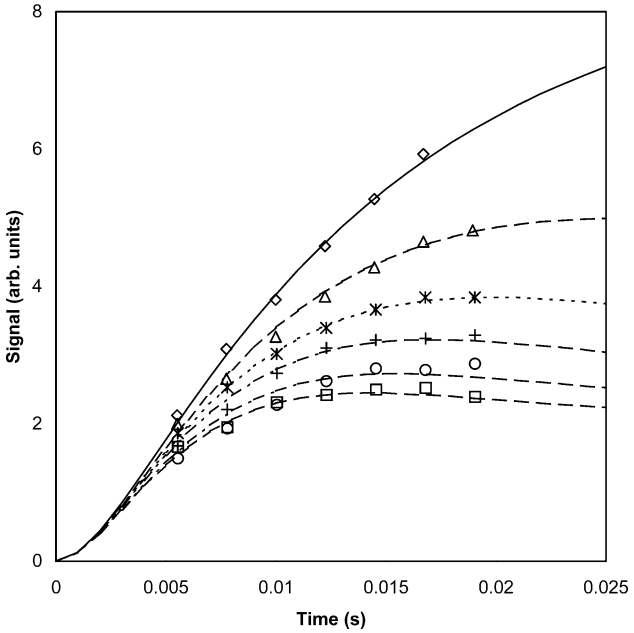

Figure 2. Variation of peroxy radical signals as a function of reaction time at different NO concentrations. Experiment conditions are P = 1.86 Torr, U = 2260 cm s^{-1}, Re = 85, [C_5H_8] = 8.4 × 10^{11} molecule cm^{-3}, [OH] = 8.8 × 10^9 molecule cm^{-3}, [O_2] = 6.8 × 10^{14} molecule cm^{-3}, and [NO] (10^{12} molecule cm^{-3}) = 0, 3.0, 6.0, 8.8, 11.8, and 14.4 for the curves from top to bottom, respectively.

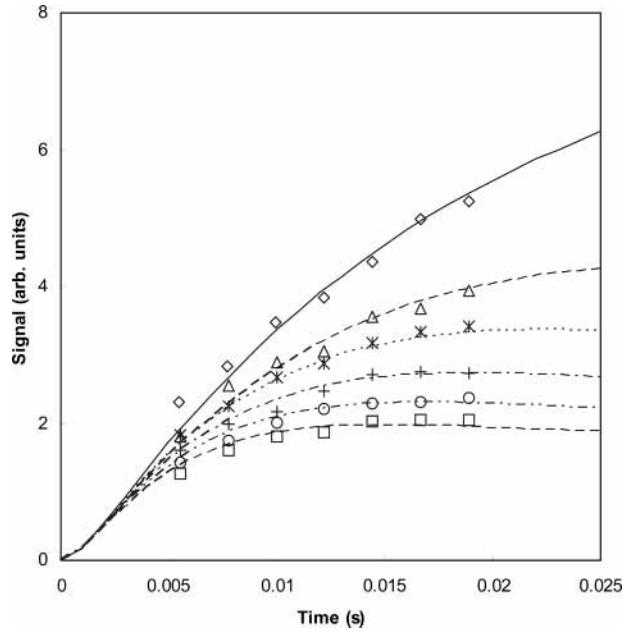

Figure 3. Variation of peroxy radical signals as a function of reaction time at different NO concentrations. Experiment conditions are P = 1.89 Torr, U = 2270 cm s^{-1}, Re =87, [C_5H_8] = 6.2 × 10^{11} molecule cm^{-3}, [OH] = 6.5 × 10^9 molecule cm^{-3}, [O_2] =1.5 × 10^{15} molecule cm^{-3}, and [NO] (10^{12} molecule cm^{-3}): 0, 2.9, 5.7, 8.7, 11.5, and 14.9 for the curves from top to bottom, respectively.

tion, the peroxy radical signal increases initially and then decreases at the longer reaction time, in contrast to the continuing increase to its equilibrium level in the absence of NO. This suggests an increasing competition between the formation and consumption of the peroxy radicals at the higher NO concentration, that is, because of the competing reactions 2 and 3. Figure 3 shows another set of data for the peroxy radical profiles with various NO concentrations: the initial isoprene and O_2 concentrations are different from those in Figure 2. Both figures reflect the similar dependence of the peroxy radical profiles on the NO concentration.

TABLE 2: Summary of Experimental Conditions for Measuring the Rate Constant for the Reaction of NO with Isoprene Hydroxy Peroxy Radicals

[C_5H_8] (molecule cm^{-3})	[O_2] (molecule cm^{-3})	[NO] (molecule cm^{-3})	[OH] (molecule cm^{-3})
8.4 × 10^{11}	6.7 × 10^{14}	0	8.8 × 10^9
8.3 × 10^{11}	6.8 × 10^{14}	3.0 × 10^{12}	8.8 × 10^9
8.4 × 10^{11}	6.8 × 10^{14}	6.0 × 10^{12}	8.8 × 10^9
8.5 × 10^{11}	6.7 × 10^{14}	8.8 × 10^{12}	8.8 × 10^9
8.3 × 10^{11}	6.8 × 10^{14}	1.2 × 10^{13}	8.8 × 10^9
8.5 × 10^{11}	6.8 × 10^{14}	1.4 × 10^{13}	8.8 × 10^9
9.5 × 10^{11}	1.1 × 10^{15}	3.2 × 10^{12}	8.2 × 10^9
9.7 × 10^{11}	1.1 × 10^{15}	5.8 × 10^{12}	8.2 × 10^9
6.2 × 10^{11}	1.5 × 10^{15}	0	6.5 × 10^9
5.8 × 10^{11}	1.5 × 10^{15}	2.9 × 10^{12}	6.5 × 10^9
6.2 × 10^{11}	1.5 × 10^{15}	5.7 × 10^{12}	6.5 × 10^9
6.2 × 10^{11}	1.5 × 10^{15}	8.7 × 10^{12}	6.5 × 10^9
6.2 × 10^{11}	1.5 × 10^{15}	1.2 × 10^{13}	6.5 × 10^9
6.2 × 10^{11}	1.5 × 10^{15}	1.5 × 10^{13}	6.5 × 10^9
5.7 × 10^{11}	1.1 × 10^{15}	9.5 × 10^{12}	5.2 × 10^9
9.0 × 10^{11}	1.1 × 10^{15}	9.5 × 10^{12}	5.2 × 10^9
1.2 × 10^{12}	1.1 × 10^{15}	9.5 × 10^{12}	5.2 × 10^9
1.5 × 10^{12}	1.1 × 10^{15}	9.5 × 10^{12}	5.2 × 10^9
1.8 × 10^{12}	1.1 × 10^{15}	9.7 × 10^{12}	5.2 × 10^9
2.3 × 10^{12}	1.1 × 10^{15}	9.3 × 10^{12}	5.2 × 10^9

To evaluate the sensitivity of fitting the peroxy radical profiles with an overall rate constant for reaction 3, we varied this rate constant in the kinetic model by ±50%, as shown in Figure 4. The three lines on the top figure represent the fittings to the observed profiles of the peroxy radical assuming three different rate constants for reaction 3, with the values of (a) 4 × 10^{-12}, (b) 9 × 10^{-12}, and (c) 1.4 × 10^{-11} cm^3 molecule^{-1} s^{-1}, respectively. Note that the simulation lines (a) and (c) are scaled to fit through the experimental data. Linear regression between the measured and simulated values was performed for the three cases (bottom figures), showing that the rate constant of 9 × 10^{-12} cm^3 molecule^{-1} s^{-1} represents the best fit to the measured peroxy radical data. The results shown in Figure 4 are typical of the experiments reported in this study.

The Experimental conditions for measuring the reaction rate constant between OH−O_2-isoprene peroxy radical and NO are summarized in Table 2. At pressures between 1 and 2 Torr, a rate constant of 9 × 10^{-12} cm^3 molecule^{-1} s^{-1} has been derived for reaction 3 at various conditions (i.e., different initial reactant concentrations and flow conditions).

We performed sensitivity analysis to assess the dependence of the kinetic simulations to variations in the RO_2 + NO rate constant. The analysis also provides information concerning the relative sensitivity of the rate constants included in the reaction mechanism. The normalized sensitivity coefficient represents the differential of jth species concentration with the ith rate constant evaluated at a fixed time in the reaction,

$$\varsigma_i = \frac{d \ln c_j}{d \ln k_i} \tag{9}$$

Figure 5 shows the sensitivity analysis based on the concentrations given in Figure 4, at a time of 18 ms which is characteristic of the reaction time in the experiment. There are two important conclusions that can be derived from the sensitivity analysis: (1) the simulations are most sensitive to the title rate constant (i.e., reaction 3) and (2) the simulations are less sensitive to most other rate constants in the oxidation mechanism in Table 1. This is particularly true for the O_2 addition rate constant (k_2) that has a large reported uncertainty (±50%).[15] Our previous

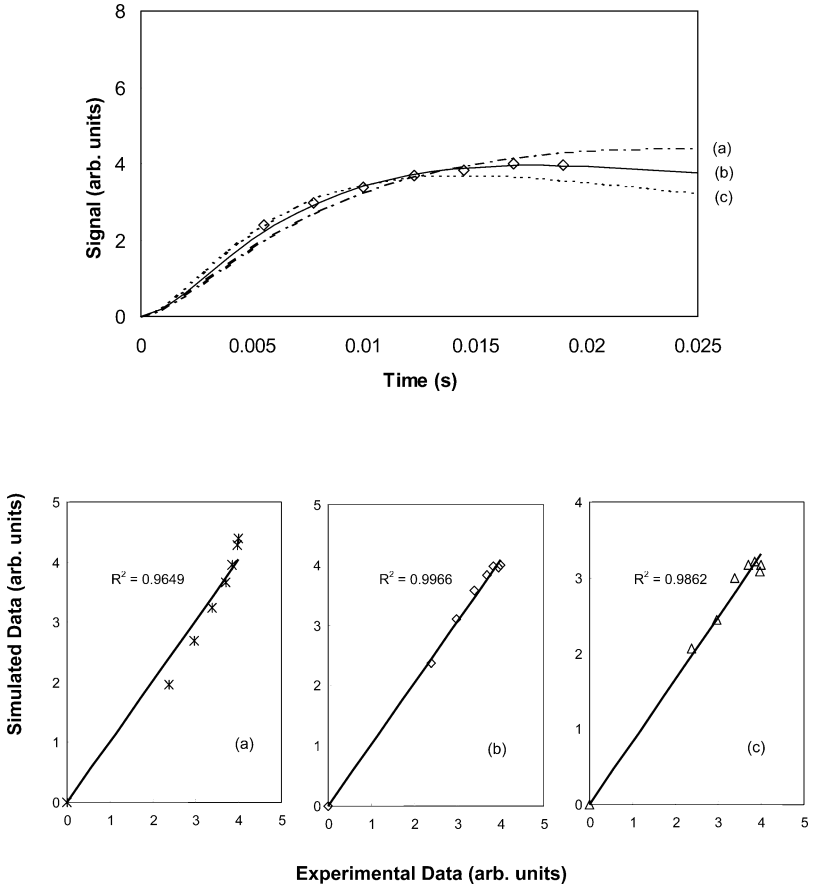

Figure 4. Time evolution of the peroxy radical signals (top). The lines represent simulations with $k_3 = 4.0 \times 10^{-12}$ (line a), 9.0×10^{-12} (line b), and 1.4×10^{-11} (line c) cm^3 molecule^{-1} s^{-1}, respectively. Simulation lines a and c are scaled to fit through the experimental data. Initial experiment conditions are $P = 1.86$ Torr, $U = 2268$ cm s^{-1}, Re = 85, $[C_5H_8] = 9.6 \times 10^{11}$ molecule cm^{-3}, $[O_2] = 1.1 \times 10^{15}$ molecule cm^{-3}, [OH] = 8.2 $\times$ 10^9 molecule cm^{-3}, and [NO] = 5.8×10^{12} molecule cm^{-3}. The bottom figures correspond to linear regression between the measured and simulated values for the three kinetic simulations with k_3 values of (a) 4.0×10^{-12}, (b) 9.0×10^{-12}, and (c) 1.4×10^{-11} cm^3 molecule^{-1} s^{-1}, respectively.

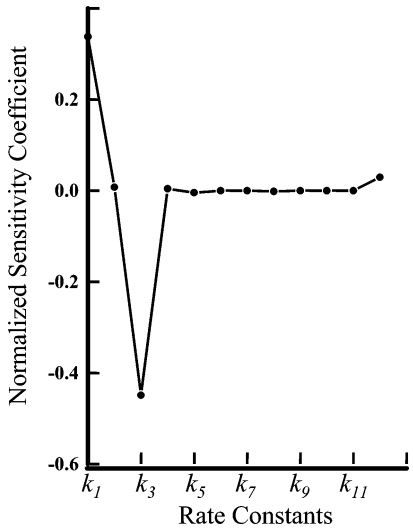

Figure 5. Normalized sensitivity coefficient as a function of rate constants in the oxidation mechanism evaluated at a time of 1.8×10^{-3} s. Rate constants $k_1 \sim k_{12}$ correspond to reactions in the order as listed in Table 1. The concentrations of NO, O_2, and C_5H_8 were 5.8×10^{12} molecules cm^{-3}, 1.1×10^{15} molecules cm^{-3}, and 9.6×10^{11} molecules cm^{-3} respectively.

study indicates that at O_2 concentrations of $(6 \sim 8) \times 10^{14}$ molecules cm^{-3} the formation profiles of the peroxy radicals are essentially nondistinguishable, as they approach an asymptotic curve defined uniquely by the isoprene and OH concentrations and the reaction time.[15] This explains that under current experimental conditions ($[O_2] > 6.7 \times 10^{14}$ molecules cm^{-3}) fitting of the experimental data is rather insensitive to the rate constant for reaction 2. Figure 5 indicates that the simulations are very sensitive to the OH−isoprene addition rate constant (k_1), with a sensitivity coefficient of about 35%. The rate constant for reaction 1 is well established with an estimated error bar of ±10%.[2] Considering the calculated sensitivity coefficient for reaction 1, the uncertainty on the rate constant of reaction 3 propagated from reaction 1 is estimated to be less than ±5%. The simulation is somewhat sensitive to the HO_2−NO rate constant (k_{12}) which determines the OH cycling, but the sensitivity coefficient is of the order of a few percents. The uncertainties on k_3 propagated from other reactions in the oxidation mechanism are negligible on our experimental time scale. Also, we estimated an additional systematic error of ±20% for this reaction in the present data, related to experimental uncertainty associated with detection of the OH−O_2−isoprene peroxy radical, the measurements of gas flows, temperature, and pressure, and in the flow considerations. Possible errors related to the background signal at $m/e = 117$ were minimal. The measured signal intensities were always higher than the background by at least 1 order of magnitude. We also considered the uncertainty associated with the determination of the OH concentration (about ±50%). To assess the sensitivity of the OH concentration on the measured rate constant for reaction 3, we varied the initial OH concentrations by ±50% in the model simulation. The result suggested that the error in OH concentration determination did not propagate noticeably into the uncertainty in the rate constant measurement for reaction

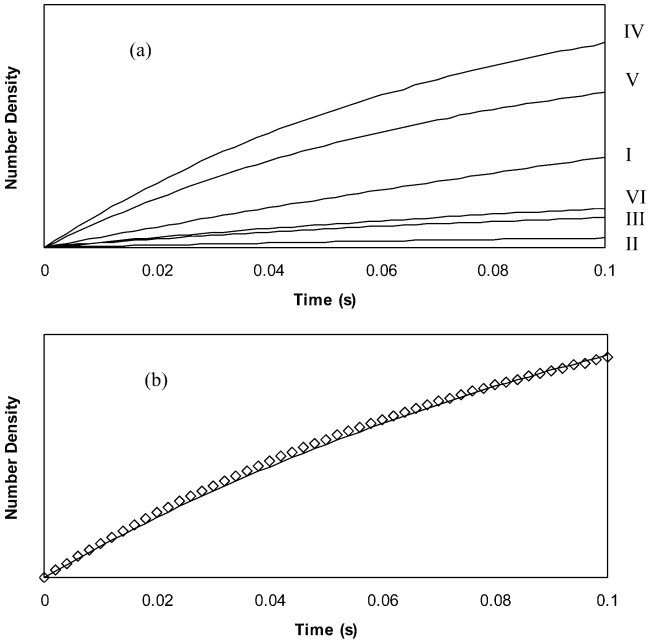

Figure 6. Simulations of peroxy radical isomer formation as a function of reaction time with the inclusion of reaction 3 on the basis of the rate constants calculated by Zhang et al.[8] The upper panel shows simulated time-dependent curves for the six distinct peroxy isomers (I−VI according to ref 8). The lower panel shows the sum of the six curves individual curves (circles) and the best effective rate constant for the RO_2–NO reaction line.

3. Hence, we estimated an overall uncertainty of ±30% in our reported rate constant for reaction 3. The CIMS method does not discriminate between isomers of the isoprene peroxy radicals. We believe that the rate constant reported in this work correspond likely to the effective rate constant of reaction 3 rather than to individual isomeric radicals.

Recently, we have reported a theoretical study of the RO_2–NO reaction using DFT and ab initio molecular orbital calculations.[8] The high-pressure limit rate constants to form ROONO were calculated by using canonical variational transition-state theory (CVTST), in the range of 3×10^{-12} to 2×10^{-11} cm^3 $molecule^{-1}$ s^{-1} for the isomers of the peroxy radicals. Hence, the isomers of the isoprene peroxy radicals exhibit distinct multiexponential kinetic behavior. As a consequence, the appearance curves for the O_2−OH−isoprene peroxy radicals consist of the sum of six appearance curves, each weighted by the branching ratio determined by both the OH and O_2 addition rate constants. Although the kinetics appears intractable, simulations suggest that the overall appearance curves of the peroxy radicals can be modeled using a single effective rate constant. Figure 6 shows the results of kinetics simulations based on the rate constants previously calculated for the six distinct peroxy radical isomers.[8] The upper panel shows the appearance curves for each peroxy isomer, which could be measured if the detection scheme permitted one to distinguish between isomers. As mentioned previously, the CIMS technique does not permit selective detection, and the experimental peroxy appearance curve represents a weighted sum of these curves. The lower panel of Figure 6 illustrates that this sum can be modeled using a single effective rate constant, with a value of 8×10^{-12} cm^3 $molecule^{-1}$ s^{-1}. The present experimental value of $(9 \pm 3) \times 10^{-12}$ cm^3 $molecule^{-1}$ s^{-1} for the RO_2−NO reaction is consistent with the theoretical predication, considering the respective uncertainties in the experimental and theoretical approaches.

The agreement between the experimentally measured rate constant at the pressure range of 1 to 2 Torr and the theoretically predicted high-pressure limit rate constant for the RO_2−NO reaction also suggests that the high-pressure limit is effectively achieved in our experimental pressure range. This is expected since the entrance and exit channels of the RO_2−NO reaction are barrierless.[8] At all energies above the entrance channel, the dissociation rate for the ROONO intermediate to form RO and NO_2 is larger than both the collision rate and dissociation rate to form RO_2 and NO.[8] In addition, the theoretically predicted barrier heights for isomerization to $RONO_2$ are in the range between 0.4 kcal mol^{-1} below and 3.7 kcal mol^{-1} above the dissociation energy of ROONO to RO and NO_2.[8]

Two previous experimental studies have investigated OH cycling from the OH-initiated reactions of isoprene in the presence of O_2 and NO, using laser-induced fluorescence for OH detection.[13,14] On the basis of the departure from the pseudo-first-order kinetics for the OH radicals, a rate constant for reaction 3 was inferred. The reported rate constants are $(1.1 \pm 0.8) \times 10^{-11}$ cm^3 $molecule^{-1}$ s^{-1} by Chuong and Stevens[13] and $(2.5 \pm 0.5) \times 10^{-11}$ cm^3 $molecule^{-1}$ s^{-1} by Reitz et al.[14] Our experimental result is within the error bar of the former value but is smaller than the latter one.[14] However, ongoing OH cycling studies in the North group have obtained a rate constant of less than the value reported by Reitz et al. for reaction 3. Our results are also consistent with the literature rate constant values for the reactions of other peroxy radicals with NO.[2,20]

The results from this study confirm that under tropospheric conditions isoprene peroxy radicals react mainly with NO, rather than engage in self- or cross-reactions (i.e., RO_2−RO_2 reactions). The fate of the resulting ROONO intermediate from the RO_2−NO reaction will be determined by several competing reaction pathways, including decomposition to RO and NO_2 or to RO_2 and NO and isomerization to the organic nitrates ($RONO_2$). Also, since the RO_2−NO reaction is exogergic, the ROONO intermediate will be produced in the vibrationally excited form, which subsequently reacts via unimolecular reactions or is collisionally stabilized. The dominant reaction pathway of the excited ROONO intermediate is prompt decomposition to RO and NO_2, along with a small fraction of prompt isomerization to $RONO_2$.[8]

4. Conclusions

We have presented the first direct experimental kinetic study of the reaction between NO and hydroxyalkyl peroxy radical arising from the OH-initiated oxidation of isoprene. Direct observation of the isoprene peroxy radical has been made using the CIMS method. By monitoring the production of the peroxy radical in the presence of NO, we have obtained the rate constant between the peroxy radical and NO. In the pressure range of 1 to 2 Torr and at 298 ± 2 K, the rate constant is $(9 \pm 3) \times 10^{-12}$ cm^3 $molecule^{-1}$ s^{-1}, where the error bar indicates the estimated systematic errors. Our present experimental results are in agreement with our recent theoretical predications of the isoprene RO_2–NO reaction using quantum-chemical methods and kinetic rate theories.[7] Under the atmospheric conditions, the reaction between isoprene peroxy radicals and NO plays an important role in tropospheric ozone formation.

Acknowledgment. This work was partially supported by the Robert A. Welch Foundation (A-1417), the Texas Advanced Research Program (ARP-Chemistry), the National Science Foundation (CH-20020), and the Environmental Protection Agency EPA (R03-0132). The authors acknowledge the assistance of Jiho Park in sensitivity analysis reported in this work

and helpful discussions with Dean Atkinson. Two referees provided valuable comments for improving the manuscript.

References and Notes

(1) Rasmussen, R. A.; Khalil, M. A. K. *J. Geophys. Res.* **1988**, *93*, 1417.

(2) Atkinson, R.; Baulch, D. L.; Cox, R. A.; Crowley, J. N.; Hampson, R. F.; Kerr, J. A.; Rossi, M. J.; Troe, J. *Summary of Evaluated Kinetic and Photochemical Data for Atmospheric Chemistry*, IUPAC, 2002. http://www.iupac-kinetic.ch.cam.ac.uk/.

(3) Chameides, W. L.; Lindsay, R. W.; Richardson, J.; Kiang, C. S. *Science* **1988**, *241*, 1473.

(4) Jacob, D. J.; Wofsy, S. C. *J. Geophys. Res.* **1988**, *93*, 1477.

(5) (a) Zhang, D.; Zhang, R. *J. Am. Chem. Soc.* **2002**, *124*, 2692. (b) Suh, I.; Lei, W.; Zhang, R. *J. Phys. Chem. A* **2001**, *105*, 6471. (c) Suh, I.; Zhang, R. *J. Phys. Chem. A* **2000**, *104*, 6590.

(6) (a) Lei, W.; Derecskei-Kovacs, A.; Zhang, R. *J. Chem. Phys.* **2000**, *113*, 5354. (b) Lei, W.; Zhang, R.; McGivern, W. S.; Derecskei-Kovacs, A.; North, S. W. *Chem. Phys. Lett.* **2000**, *326*, 109. (c) Lei, W.; Zhang, R.; McGivern, W. S.; Derecskei-Kovacs, A.; North, S. W. *J. Phys. Chem. A* **2001**, *105*, 471.

(7) Paulson, S. E.; Seinfeld, J. H. *J. Geophys. Res*. **1992**, *97*, 20703.

(8) Zhang, D.; Zhang, R.; Park, J.; North, S. W. *J. Am. Chem. Soc*. **2002**, *124*, 9600.

(9) Wiedinmyer, C.; Friedfeld, S.; Baugh, W.; Greenberg, J.; Geunther, A.; Fraser, M.; Allen, D. *Atmos. Environ.* **2001**, *35*, 1001.

(10) Chen, X. H.; Hulbert, D.; Shepson, P. B. *J. Geophys. Res.* **1998**, *103*, 25563.

(11) Horowitz, L. W.; Liang, J.; Gardner, G. M.; Jacob, D. J. *J. Geophys. Res.* **1998**, *103*, 13451.

(12) Zhang, R.; Suh, I.; Lei, W.; Clinkenbeard, A. D.; North, S. W. *J. Geophys. Res*. **2000**, *105*, 24627.

(13) Chuong, B.; Stevens, P. S. *J. Geophys. Res.* **2002**, *107*, art. no. 4162.

(14) Reitz, J. E.; McGivern, W. S.; Church, M. C.; Wilson, M. D.; North, S. W. *Int. J. Chem. Kinet.* **2002**, *34*, 255.

(15) Zhang, D.; Zhang, R.; Church, C.; North, S. W. *Chem. Phys. Lett*. **2001**, *343*, 49.

(16) Tuazon, E. C.; Atkinson, R. *Int. J. Chem. Kinet.* **1990**, *22*, 1221.

(17) Sprengnether, M.; Demerjian, K. L.; Donahue, N. M.; Anderson, J. G. *J. Geophys. Res.* **2002**, *107*, Art. No. 4269.

(18) Stevens, P.; L'Esperance, D.; Chuong, B.; Martin, G. *Int. J. Chem. Kinet.* **1999**, *31*, 637.

(19) Jenkin, M. E.; Boyd, A. A.; Lesclaux, R. *J. Atmos. Chem.* **1998**, *29*, 267.

(20) (a) Eberhard, J.; Howard, C. *J. Phys. Chem. A* **1997**, *101*, 3360. (b) Eberhard, J.; Howard, C. J. *Int. J. Chem. Kinet.* **1996**, *28*, 731. (c) Eberhard, J.; Villalta, P. W.; Howard, C. J. *J. Phys. Chem. A* **1996**, *100*, 993. (d) Villalta, P. W.; Huey, L. G.; Howard, C. J. *J. Phys. Chem. A* **1995**, *99*, 12829.

(21) Suh, I.; Zhang, R. *J. Phys. Chem. A* **2000**, *104*, 6590.

(22) Suh, I.; Lei, W.; Zhang, R. *J. Phys. Chem. A* **2001**, *105*, 6471.

(23) Keyser, L. F. *J. Phys. Chem.* **1984**, *88*, 4750.

(24) Zhang, R.; Molina, L. T.; Molina, M. J. *Rev. Sci. Instrum*. **1998**, *69*, 4002.

(25) Zhang, R.; Lei, W.; Molina, L. T.; Molina, M. J. *Int. J. Mass Spetrom.* **2000**, *194*, 41.

(26) DeMore, W. B.; Sander, S. P.; Howard, C. J.; Ravishankara, A. R.; Golden, D. M.; Kolb, C. E.; Hampson, R. F.; Kurylo, M. J.; Molina, M. J. *Chemical Kinetics and Photochemical Data for Use in Stratospheric Modeling*, JPL Pub. 97−4, NASA, Jet Propul. Lab.: Pasadena, CA, 1997.

(27) Zhang, R.; Lei, W. *J. Chem. Phys.* **2000**, *113*, 8574.

(28) Dibble, T. S. *J. Phys. Chem. A* **1999**, *103*, 8559.

(29) Lei, W.; Zhang, R. *J. Phys. Chem. A* **2001**, *105*, 3808.